Iranian Journal of Physics Research, Vol. 25, No. 3, 2025
DOI: 10.47176/ijpr.25.3.81967

Investigation of the effect of cold atmospheric pressure He plasma on the electrochemical hydrogen storage performance of Co/MWCNT nanoelectrodes

Maryam Malmir[1,*], Azadeh Barjasteh[1] and Shokufeh Varshoy[2]
[1] Department of Physics, Lorestan University, Khorramabad 68151-44316, Iran;
[2] University of Technology Sydney

E-mail: malmir.m@lu.ac.ir

(Received 28 August 2024 ; in final form 09 January 2025)

Abstract
The effect of cold atmospheric *He* plasma on multi-walled carbon nanotube (MWCNT) / cobalt nanoelectrodes has been investigated for reversible hydrogen ion storage. To perform plasma treatment, the material suspensions were subjected to plasma treatment for different durations, such as 30, 60, and 100 seconds, and then deposited on Cu foam to be used as active anode material. After characterization, the discharge capacity of the nanoelectrodes was examined, revealing that cold plasma treatment, even at the shortest duration (30 seconds), increases the hydrogen storage capacity of the nanoelectrodes due to the formation of reactive oxygen and nitrogen functional groups on the walls of the MWCNTs. This study also indicated that there is an optimal plasma treatment time of 60 seconds, resulting in the highest discharge capacity of 9700 mAh/gr at a constant current of 1 mA. Consequently, *He* plasma treatment of the nanoelectrodes offers promising applications in hydrogen storage and the battery industry.

Keywords: Cold Plasma, Electrochemical Hydrogen Storage Capacity, MWCNT / Cobalt nanoelectrode.

1. Introduction

One of the principal issues in the economic development of countries is clean and sustainable energy, due to the increasing need for energy resulting from population growth. The growth of the world population and the increasing use of natural energy resources, such as fossil fuels, have caused the world to face a serious reduction in these resources and climate change. These problems have increased the demand for clean and sustainable energy to replace fossil fuels. Studies in recent years have shown that hydrogen-based fuel cells are the best alternative energy source because they are produced effortlessly, have high energy density, and can be easily converted to other forms of energy, such as convenient fuel for transportation [1-5]. In these fuel cells, electricity is produced by combining hydrogen and oxygen, which provides a clean energy source without any air pollutants, as the only by-product is water. While hydrogen is an effective fuel that can replace fossil fuels, there are challenges, such as a lack of efficient and inexpensive methods for reversibly storing hydrogen for commercial implementation [6]. Therefore, in recent years, researchers have investigated different methods to store hydrogen, such as high pressure (compressed hydrogen), low temperature (liquid hydrogen), and porous solid materials [7-9]. The first two methods are commercially inefficient, while the last one shows promising results due to its high-capacity storage, safety, effectiveness, and low cost. Various studies have shown that carbon-based materials can store hydrogen [10-14] as a result of physical binding between hydrogen and carbon atoms. Consequently, the desorption of physisorbed hydrogen from these materials requires high activation energy. These materials also have a high surface area and low production costs; as a result of the Chahine rule, the amount of stored hydrogen is proportional to the surface area [16]. Carbon nanotubes are carbon-based materials that, in addition to the aforementioned properties, have low weight and high chemical and thermal stability for hydrogen storage. They are classified into two main groups: single-walled carbon nanotubes (SWCNT) and MWCNT. In 1997, the first study of SWCNTs showed that these particles have a high reversible hydrogen storage capacity via a physisorption mechanism due to their unique characteristics, such as a cage-like structure, high surface area, high electrical conductivity, and nonporous structure, which are necessary for dissociating hydrogen molecules and preventing carrier recombination [6, 18]. Different reports have shown that hydrogen can be stored at various sites in carbon nanotubes (CNTs), such as the outer walls, defect sites, and the spaces between single layers in MWCNTs or mesoporous tube-

like channels [19-23]. As a result, the hydrogen storage capacity in MWCNTs is significantly greater than in SWCNTs. Other studies have shown that the hydrogen storage capacity of CNTs can be increased when they are decorated with metals such as Co, Fe, Ni, and Ca [23-25]. This is because, initially, Kubas interaction enhances the adsorption of hydrogen molecules, and then hydrogen molecules are dissociated on the metal particles. Consequently, atomic hydrogen spills over into the spaces between carbon layers in MWCNTs, resulting in an increased hydrogen uptake capacity of the CNT composite [23, 26-28]. In 2010, Gao et al. showed that oxygen treatment of carbon nanotubes (CNTs) can produce defects, and doping them with metals such as Pd and Ni as catalysts can significantly increase their hydrogen storage capacity [29] .Regarding the properties of plasma, it appears that cold atmospheric pressure plasma can be used to enhance the cycle life of MWCNT-based materials decorated with metals through hydrogen adsorption at defect sites, Co nanoparticles, and the formation of oxygen-containing groups. Plasma, which is the fourth state of matter, consists of electrons, ions, excited species, free radicals, UV radiation, and electromagnetic fields. Based on species temperature, plasma is classified into two main groups: thermal plasma and non-thermal plasma. In thermal plasmas, the electron and ion temperatures are nearly the same ($T_e \approx T_{ion} \geq 10^4 K$) while in non-thermal plasmas, the electron temperature is higher than the ion temperature (with ions remaining at room temperature) $T_e (\approx 10^4 K) \gg T_{ion} (\approx 300 K)$. While the main drawback of thermal plasma is its high temperature and low excitation selectivity [30], non-thermal plasmas, such as plasma jets, have low temperatures and high excitation selectivity. Therefore, non-thermal plasmas are extensively used in industrial applications because of their high selectivity in plasma chemical reactions and their low temperature [31-33]. One of the gases commonly used as a feed gas in plasma discharges, due to its easier ignition, is *He* gas.

According to our knowledge, no hydrogen storage study has used *He* plasma treatment to investigate the effect of cold plasma treatment on the hydrogen storage capacity of composites made of Co/MWCNT. Therefore, in this study, a helium plasma jet was used before the deposition of cobalt/MWCNT on Cu foam, and the nanoelectrodes were utilized as active anode materials to investigate hydrogen storage capacity. Regarding plasma properties, an increase in hydrogen adsorption by the electrodes is expected because *He* cold plasma treatment alters the chemical surface properties of Co/MWCNT nanoelectrodes by forming functional groups such as oxygen and nitrogen on the walls of the MWCNTs. Consequently, we applied plasma at different treatment times, such as 0 seconds, 30 seconds, 60 seconds, and 100 seconds, and found that 60 seconds of plasma treatment increases hydrogen storage more effectively.

2. Experimental method

2.1 Purification

For this study, MWCNTs were synthesized using chemical vapor deposition along with molybdenum catalysis to create Co/MWCNT nanoelectrodes [34]. Their diameter was 30-40 nm. To achieve purified and functionalized MWCNTs, we treated the surface of the MWCNTs by ultrasonicating them in a mixture of H_2SO_4 and HNO_3 (1:3 volume ratio) for 4 hours at 50 °C. This chemical oxidation process produces oxygen-containing groups on the surface of the MWCNTs, resulting in increased chemical activity [35-37]. The resulting MWCNTs were then thoroughly rinsed several times with deionized water to achieve a neutral pH of 7. Finally, the purified and functionalized MWCNTs were dried at 100 °C for 3 hours. As a result, carboxylic functional groups were attached to the surface of the MWCNTs, causing them to be uniformly dispersed in the solution [38, 39].

2.2 Preparation of electrodes

The electrodeposition method was used to deposit Co/MWCNT nanoelectrodes on nanosized porous and small (1×2 cm^2) Cu foam. To carry out this process, the electrochemical bath solution consisted of 312 g L^{-1} $CoSO_4 \cdot (H_2O)_2$, 6.19 g L^{-1} NaCl, 100 g L^{-1} H_3BO_3, 0.005 g CTAB, and 0.005 g of functionalized MWCNT powder in 50 cc of double-distilled water, which were homogenized by ultrasonic vibration for 3 hours at 70 °C and stirred at room temperature for 0.5 hours. To investigate the effect of cold atmospheric pressure plasma (CAP) on the hydrogen storage capacity of the prepared electrodes, we divided the suspensions into four groups and treated them with a helium plasma jet at different exposure times of 0, 30, 60, and 100 seconds. The helium plasma jet was created using a tungsten wire inserted at the center of a quartz cylinder as a dielectric, with a copper tape used as the outer electrode. It was ignited at a rectangular voltage of 5 kV and a frequency of 20 kHz, with a gas flow rate of 1 L/min. The distance between the plasma jet nozzle and the surface of the suspension was about 2 cm. To ensure that plasma particles reached all parts of the suspension, we stirred the suspension during plasma treatment at 25 °C and 300 rpm using a magnetic stirrer. Following this, the plasma-treated suspension was used for the electrodeposition process of the electrodes. The electrodeposition was carried out using a platinum (Pt) plate as the cathode and Cu foam as the anode, separated by a gap of 1 cm, with a current density of 5 mA cm^{-2} and a duration of 5 minutes. As a result, Co/MWCNT nanoelectrodes on the Cu foam were obtained as working electrodes. Figure 1 shows a schematic summary of the experimental process.

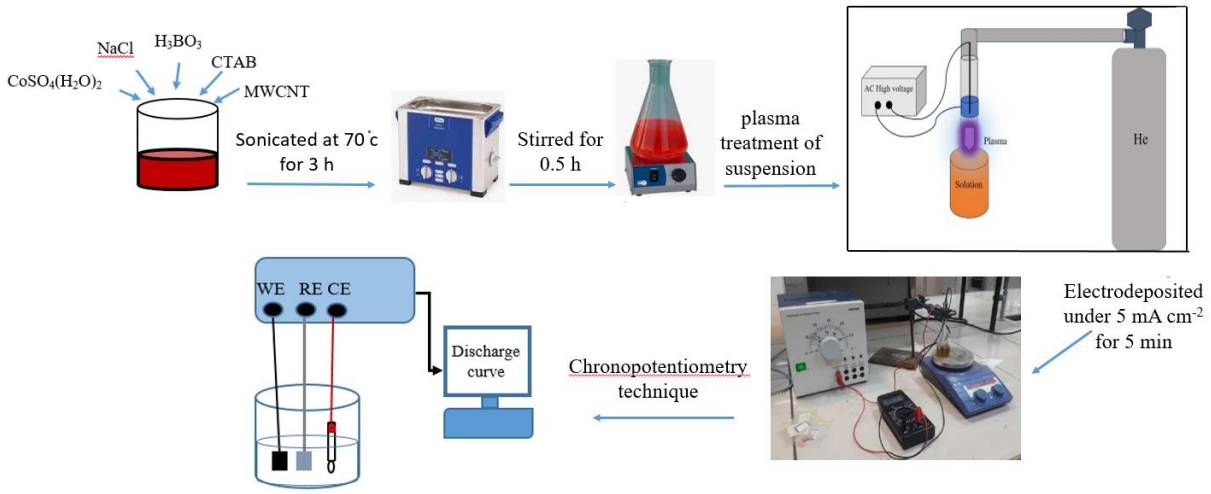

Figure 1. Schematic summary of the experimental process.

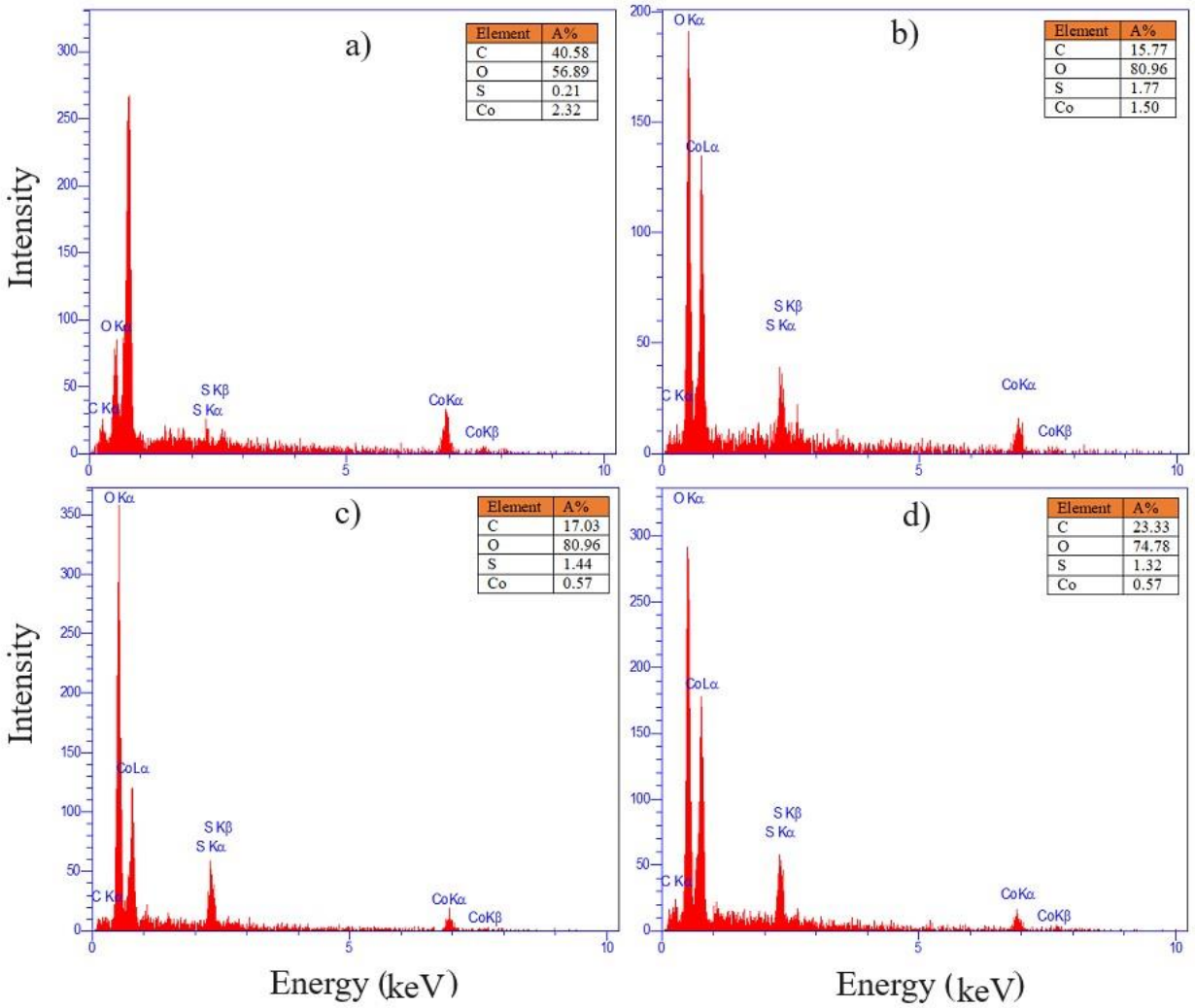

Figure 2. EDX analysis of Co/MWCNT nanoelectrodes under plasma radiation for (a) 0s (b) 30s, (c) 60s, (d) 100s.

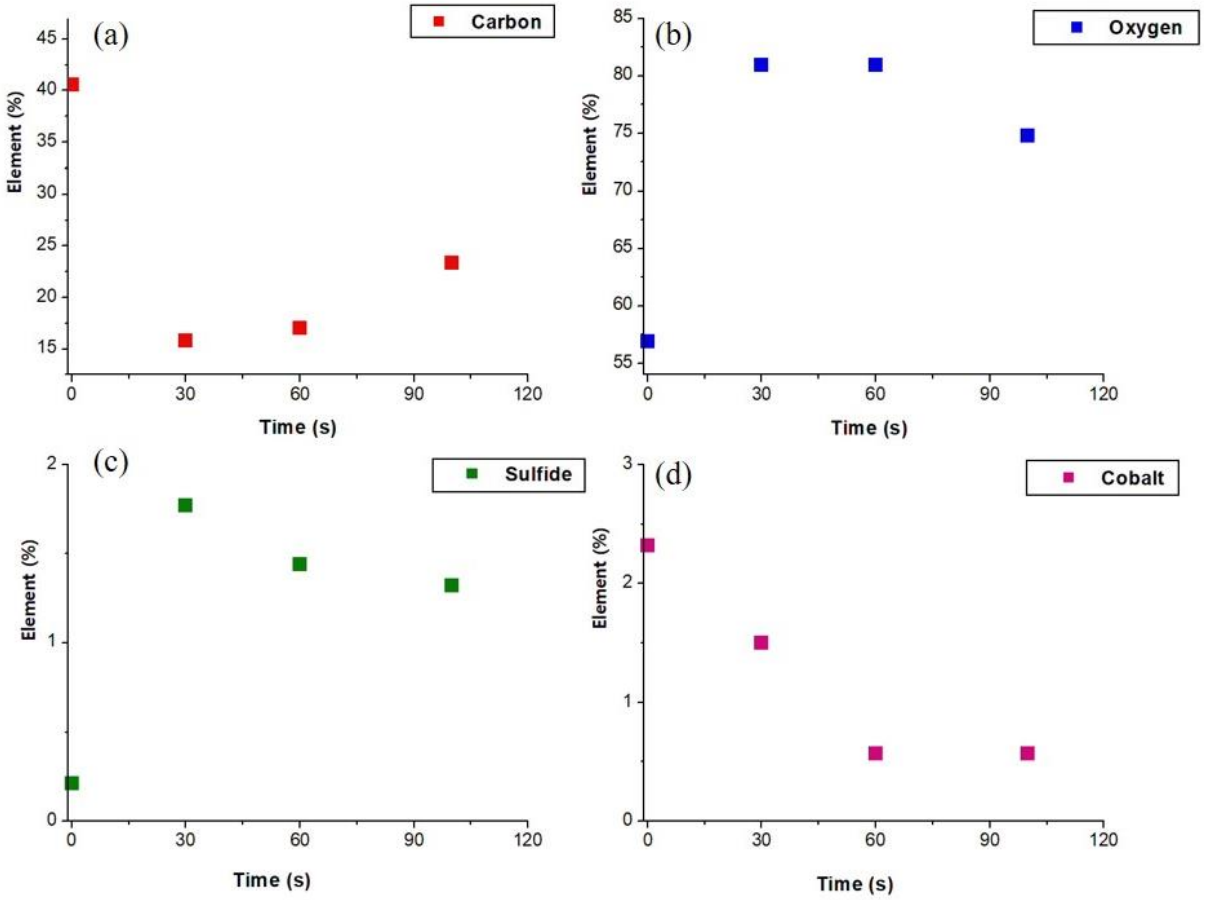

Figure 3. (a-d) Percentage of different elements (%) versus plasma radiation time.

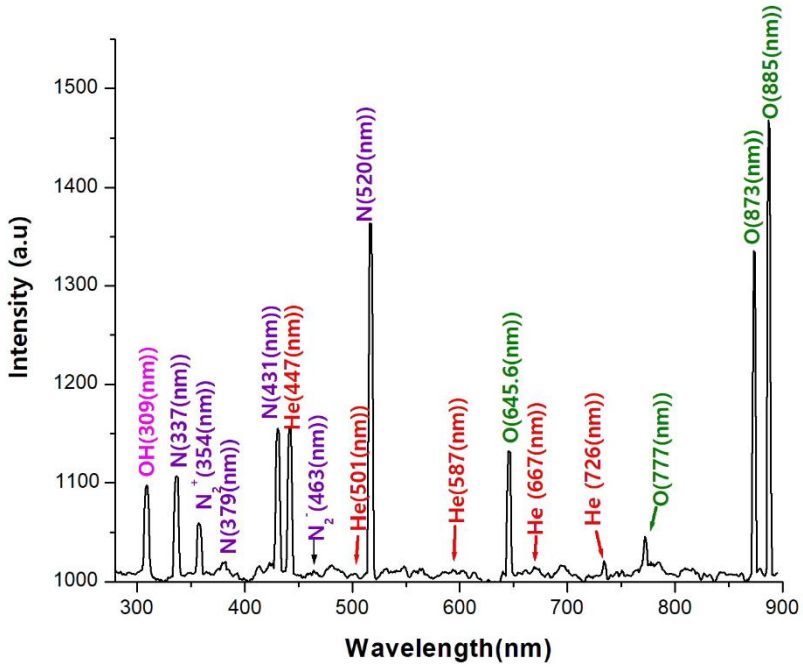

Figure 4. Spectrum produced by the He plasma jet.

2.3 Hydrogen ion storage capacity measurement

The chronopotentiometry technique was employed to perform all the chemical analyses using three-electrode cells. Pt, Ag/AgCl, and Co alloy/MWCNT were used as the counter, reference, and working (active anode material) electrodes, respectively. A liquid composed of 6 M KOH in 100 mL of deionized water was used as the electrolyte (figure 1). In this technique, a constant current of 1 mA was applied between the working and counter electrodes, and the resulting potential was measured against the reference electrode as a function of time. Finally, the electrochemical adsorption/desorption properties of the working electrodes were evaluated for the first fifteen cycles, and the storage capacity of the working electrodes was calculated using equation (1):

Specific capacity (mAh/gr) = [Constant current (mA) × Discharge time (h)] / Active material weight (g) (1)

In fact, the copper foam is weighed before and after the material is deposited onto it, and the difference is considered to be the weight of the active material weight. In this study, H^+ ions were absorbed (extracted) into the working electrode to perform charge (discharge) on the anode, based on the half-cell reaction.

3. Results and discussion

In plasma treatment, various parameters, such as plasma radiation time, gas flow rate, and gas mixture composition, affect the treatment process. In this study, the effect of plasma radiation time on the hydrogen storage capacity of Co/MWCNT nanoelectrodes has been investigated. To examine the impact of different plasma treatment times on the elemental composition of Co/MWCNT nanoelectrodes and the stoichiometric ratio of products, we employed EDX analysis. As shown in figure 2, all samples consist of different ratios of carbon (C), oxygen (O), sulfur (S), and cobalt (Co) due to receiving varying amounts of plasma radiation.

For further insight into the changes induced by cold plasma radiation, we have plotted the percentage of each element present in the EDX spectra against different plasma radiation times.

As we can see in figure 3, compared to the sample without plasma treatment (0 s), all treated samples with He plasma exhibit a lower percentage of carbon and cobalt elements while showing a higher percentage of oxygen. This observation may be attributed to the different interactions between plasma reactive species and the solution, as these reactive species activate the solution prior to layer deposition on the surface of the electrode. The 30 s and 60 s treatments with He plasma result in the highest amounts of oxygen-containing functional groups on the electrodes. These functional groups enhance the hydrophilicity and charge storage capacity of MWCNT-containing electrodes, creating active sites that are favorable for increasing hydrogen storage capacity [41]. In contrast, the 100 s treatment leads to the detachment of cobalt particles from the surface of the electrode and damages its structure. This is detrimental to both the oxidation of MWCNTs and hydrogen storage, as cobalt acts as a catalyst that promotes MWCNT oxidation, thereby increasing their hydrophilicity and charge storage capacity [23]. Concerning figure 3 (b, d), we can see that during plasma treatment from 60 to 100 s, the amount of oxygen in the samples is reduced while the cobalt amount remains nearly constant. This result indicates that other oxygen fragments may be formed from oxygen mixtures or that some portions of radicals in the plasma-treated solution have been scavenged [41]. Additionally, the decrease in cobalt particles in MWCNTs leads to reduced adsorption and dissociation of hydrogen atoms, resulting in a decreased hydrogen storage capacity. To gain more insight into the reactive species present in the He plasma jet, optical emission spectroscopy was employed during solution treatment, measured by an ISTA-UV spectrometer. The tip of the optical fiber is placed directly in front of the plasma nozzle to record the plasma spectrum. This spectrum is shown in figure 4. As we can see in this figure, hydroxyl radicals, as well as He, nitrogen, and oxygen reactive species, are identified. These reactive species interact with the solution to produce other reactive species that can create defects on the walls of carbon nanotubes.

These defects, which are high-energy sites, are suitable for binding oxygen-containing functional groups such as O-H, C-O, and C-O-N. The presence of these oxygen functional groups was previously confirmed in the EDX images shown in figures 2 and 3 [41]. Therefore, as a result, plasma treatment in all samples increased the oxygen functional groups through the production of reactive oxygen species such as OH; however, with increasing treatment time, the amount of oxygen decreased. The functional groups enhance the hydrogen storage capacity of MWCNTs through two main mechanisms: (i) the creation of pores on a nanometer scale, which increases the surface area and creates deep potential wells, and (ii) doping with elements that can enhance hydrogen interaction [42-44].

To investigate the structural changes of samples treated by the *He* plasma jet at different treatment times, we employed X-ray diffraction (XRD) analysis using the X/Pert Pro system, as shown in figure 5. All diffraction peaks of cobalt correspond to the hexagonal form of cobalt. Figure 5(a) shows the XRD pattern of the sample with no plasma treatment and confirms the formation of a Co/MWCNT nanoelectrode, evidenced by the appearance of hexagonal carbon and cobalt peaks. The highest peak in this figure is attributed to the hexagonal carbon nanotube peak. By comparing figures 5 (b), (c), and (d), we can see that as the plasma radiation time increases from 0 to 100 s, the intensity of the carbon and cobalt hexagonal peaks decreases as a result of the activation of the solution by plasma reactive species. As previously shown in figure 4, the plasma consists of different reactive species, such as reactive oxygen, nitrogen, and helium species, which, upon contact with the aqueous solution, produce additional reactive species. In contact with the aqueous solution, long-lived reactive species such as H_2O_2, O_3, NO_2^-, and NO_3^- are produced alongside short-

lived reactive species such as OH, NO, and $ONOO^-$ [45, 46]. The long-lived reactive species remain in the solution for minutes to days, while the short-lived species persist for one nanosecond to several seconds and react quickly to produce additional long-lived species [47, 48]. These species alter the physical and chemical properties of carbon nanotubes by introducing oxygen groups on their surfaces. Various reports have shown that with increasing treatment time, the physicochemical properties of the treated solution such as density, concentration of reactive species, oxidation-reduction potential, and conductivity increase [49-51]. Additionally, as shown in figure 5 (b), in the sample with 30 s of plasma treatment, carbon appears in the cubic phase instead of the nanotube phase due to the introduction of reactive oxygen-containing functional groups into the structure of MWCNTs [52] . As demonstrated in Ref. [50], with increasing plasma treatment time, the amounts of oxygen and nitrogen groups significantly increase in the solution. These functional groups are incorporated into MWCNTs by interacting with OH radicals in the aqueous solution, allowing CNTs to store charge through surface reversible redox reactions, thereby facilitating a pseudo-capacitive mechanism and increasing the electrode's capacitance [53-55]. By comparing the results obtained from EDX and XRD (figures 2 and 5), one can observe a correlation between the decrease in cobalt and carbon species due to the attachment of oxygen-containing groups to the nanotubes.

Figure 6 (a-d) shows the SEM analysis of Co/MWCNT nanoelectrodes before and after plasma treatment. These figures indicate the structural properties of the samples.

As we can see in this figure, plasma treatment causes the breakdown of MWCNT agglomerations in the composite, which is an important factor for supercapacitor electrodes [41]. This breaking mechanism occurs such that after layer deposition on the surface of Cu, the nanotubes are separated from the surface and take on a net-like shape. This result also emphasizes the decrease in carbon content in the samples treated by plasma radiation, which was evident in the EDX figures. Figure 6 illustrates a net-like shape of MWCNTs in the 60 s plasma treatment, which is more effective compared to the 100 s treatment, while plasma treatment at 30 s does not produce such changes. Finally, to investigate the effect of plasma radiation on the hydrogen storage capacity of Co/MWCNT nanoelectrodes, we conducted chronopotentiometry analysis. During the charging process, electrons move to the working electrode, allowing H^+ ions to adsorb on the surface of the active electrode via physisorption. In contrast, during the discharge process, the adsorbed hydrogen on the surface of the active electrode is released [56]. As a result, the greater the amount of hydrogen adsorbed, the higher the discharge capacity. Figure 7 (a-d) illustrates the discharge behavior of the samples treated with *He* cold plasma at different times: 0 s, 30 s, 60 s, and 100 s under a constant current of 1 mA. The optimized discharge capacity of each sample can be extracted from the potential versus discharge capacity curves. In each considered sample, an increase in discharge capacity is observed with an increasing cycle number. For example, in figure 7 (a), the 15th cycle exhibits a higher discharge capacity than the first cycle due to the increased number of activated sites available for adsorbing hydrogen ions, which accounts for the greater discharge capacity. As shown in figure 7, the discharge capacities are 6711 mAh/gr, 8000 mAh/gr, 9700 mAh/gr, and 6088 mAh/gr for the 0 s, 30 s, 60 s, and 100 s samples, respectively. These results indicate that plasma treatment increases discharge capacity from 0 s to 60 s; however, increasing the treatment time to 100 s results in a decrease in discharge capacity. Consequently, the 60 s treatment with *He* cold plasma yields the highest discharge capacity, while longer treatment times have a detrimental effect on the discharge capacity of the samples. The increase in discharge capacity with plasma treatment can be attributed to the creation of novel sites such as oxygen-containing groups and the breakdown of MWCNT agglomerations, which are favorable for hydrogen adsorption. Therefore, the 60 s plasma radiation on Co/MWCNT nanoelectrodes enhances their suitability as composites for hydrogen storage applications.

4. Conclusion.

In this study, we treated the Co/MWCNT nanoelectrode with a cold atmospheric He plasma jet before layer deposition. Various plasma treatment times, such as 0 s, 30 s, 60 s, and 100 s, were applied to achieve the optimal conditions for the hydrogen storage process. Our results showed that plasma treatment, even for a short time interval such as 30 s, increases hydrogen discharge capacity by creating defects and functional groups on the surface of MWCNTs that are favorable for hydrogen storage. Based on our findings, the 60 s plasma treatment resulted in the highest discharge capacity and, consequently, the greatest hydrogen storage capacity due to the increased formation of oxygen functional groups that create defects on the walls of MWCNTs and lead to net-like shapes. However, increasing the plasma treatment time to 100 s decreases hydrogen discharge capacity due to the reduction of oxygen groups caused by the formation of other oxygen fragments or the scavenging of some radicals in the plasma-treated solution.

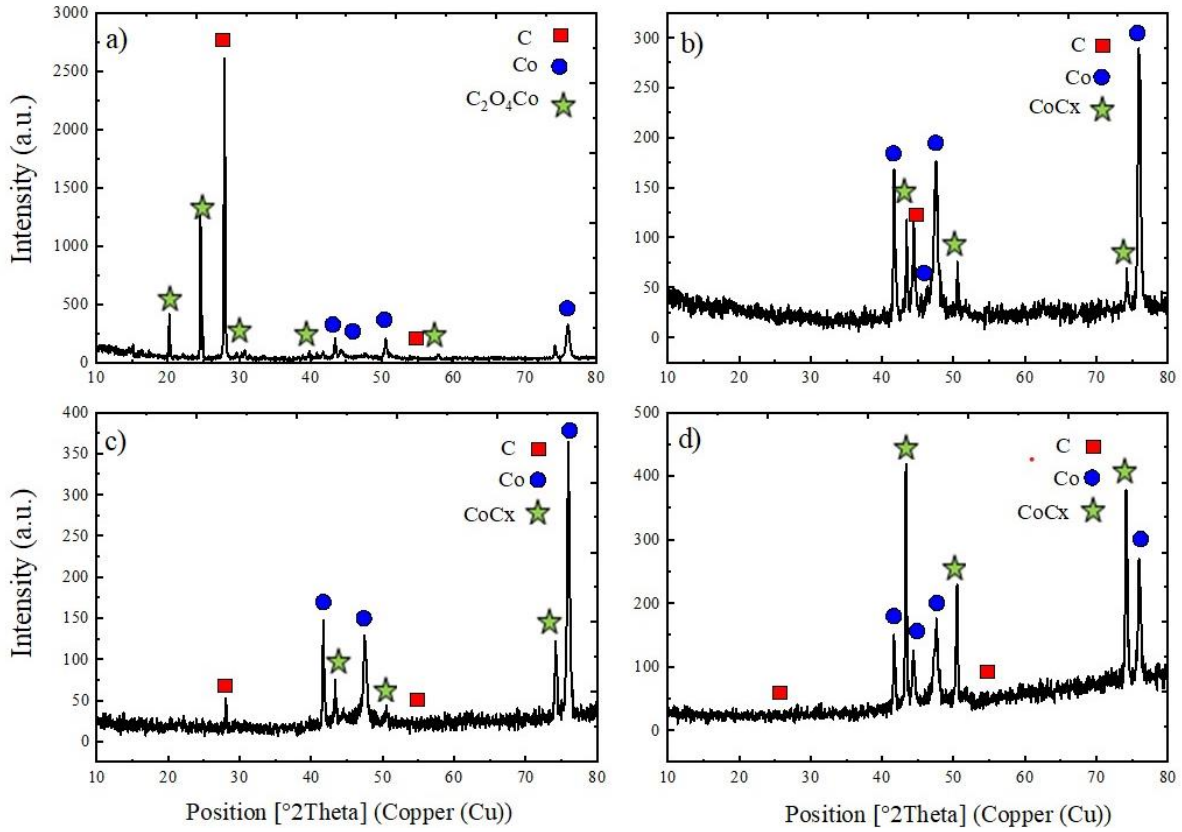

Figure 5. XRD analysis of samples irradiated by the He plasma jet at different treatment times: (a) 0 s, (b) 30 s, (c) 60 s, and (d) 100 s.

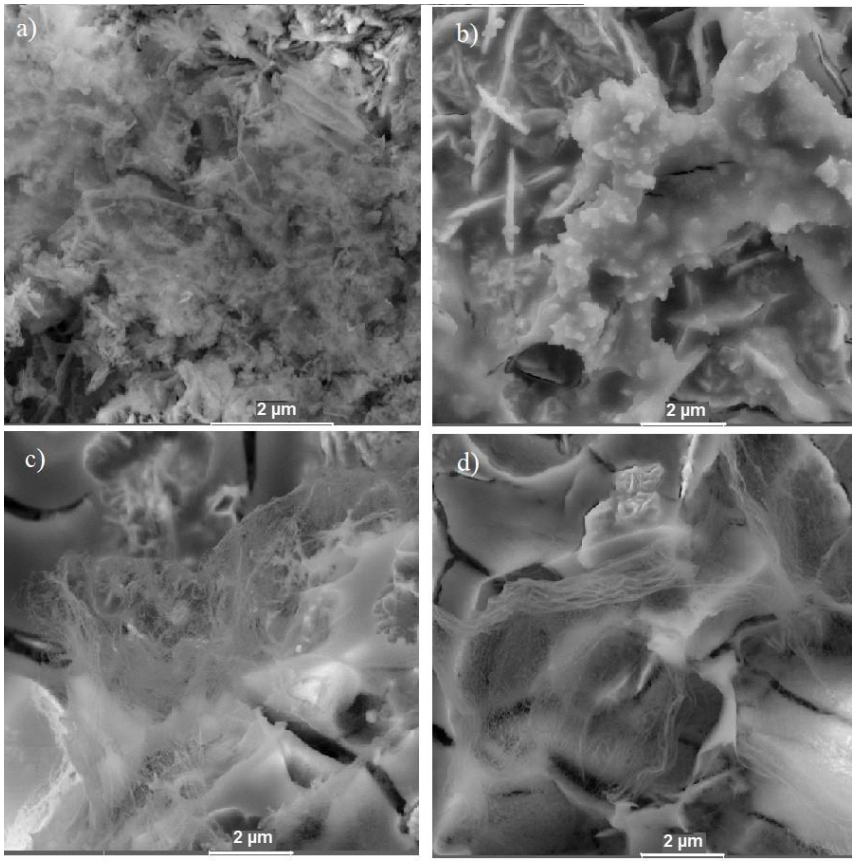

Figure 6. SEM image of analysis of irradiated Co/MWCNTs composite by He plasma jet at different treatment times (a) 0s, (b) 30s, (c) 60s, and (d) 100s.

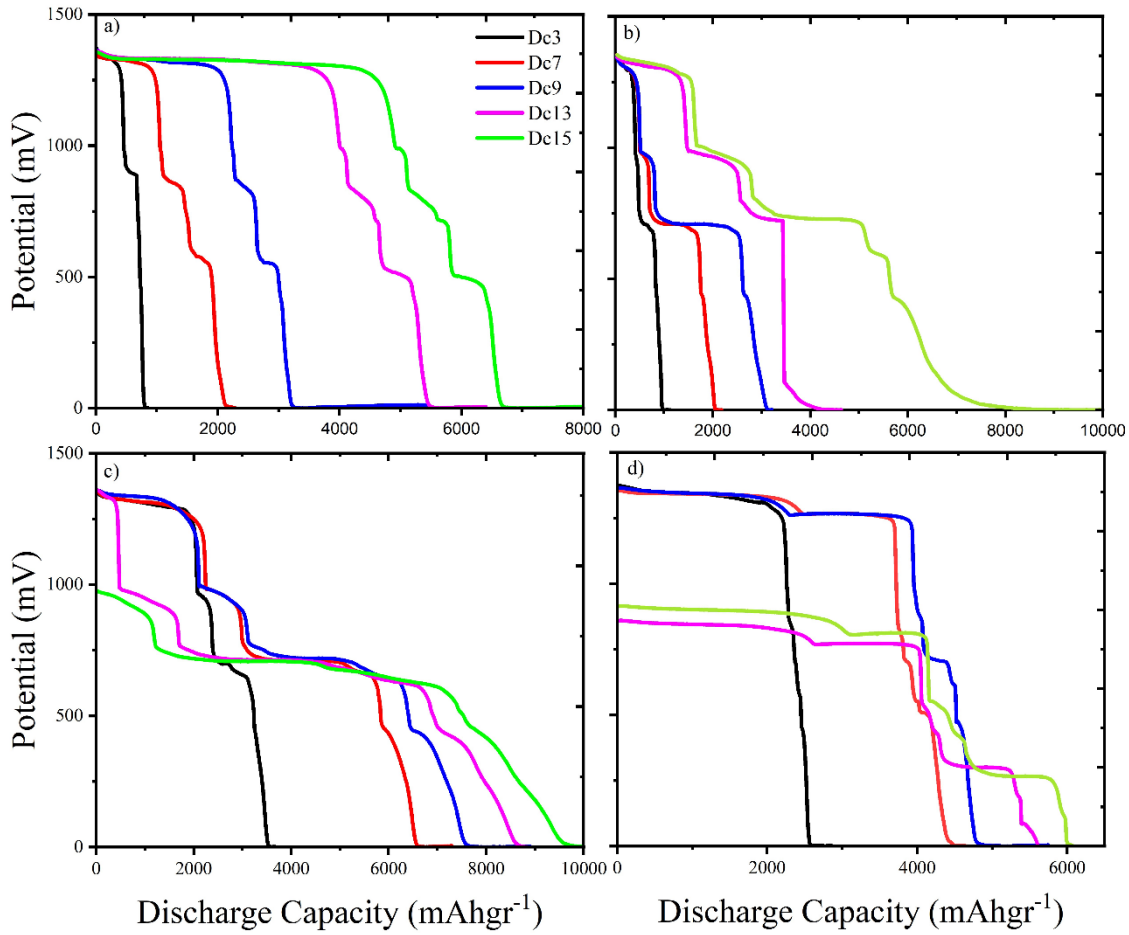

Figure 7. The hydrogen discharge capacity curves of the Co/MWCNT nanoelectrodes irradiated by He plasma jet at different treatment times (a) 0s, (b) 30s, (c) 60s, and (d) 100s.

References

1. HM Cheng, QH Yang, and C Liu, *Carbon*, **39**(10) (2001) 1447.
2. B Zohuri, *Hydrogen Energy: Challenges and Solutions for a Cleaner Future*, Springer (2019).
3. JO Abe, A Popoola, E Ajenifuja, and OM Popoola, *International Journal of Hydrogen Energy*, **44**(29) (2019)15072.
4. K Dai, L Lu, C Liang, L Geng, and G Zhu, *Materials Letters*, **176** (2016) 42.
5. AC Dillon, KEH Gilbert, PA Parilla, JL Alleman, GL Hornyak, KM Jones, and MJ Heben, *Proceedings of the 2002 US DOE Hydrogen Program Review* (2002).
6. S Ullah Rather, *International Journal of Hydrogen Energy*, **45**(7) (2020) 4653.
7. L Schlapbach, and A Züttel, *Nature*, **414**(6861) (2001) 353.
8. A Dillon, and M Heben, *Applied Physics A*, **72** (2001) 133.
9. M Hirscher, *Handbook of Hydrogen Storage: Topics in Applied Physics*, Springer (2010).
10. H Lee, J Ihm, M L Cohen, and S G Louie, *Nano Letters*, **10**(3) (2010) 793.
11. B Kuchta, L Firlej, A Mohammadhosseini, P Boulet, M Beckner, J Romanos, and P Pfeifer, *Journal of the American Chemical Society*, **134**(36) (2012) 15130.
12. L Chen, K Xia, L Huang, L Li, L Pei, and S Fei, *International Journal of Hydrogen Energy*, **38**(8) (2013) 3297.
13. M Konni, N Narayanan, AS Dadhich, and SB Mukkamala, *Fullerenes, Nanotubes and Carbon Nanostructures*, **23**(9) (2015) 782.
14. YJ Han, and SJ Park, *Applied Surface Science*, **415** (2017) 85.
15. AC Dillon, T Gennett, JL Alleman, KM Jones, PA Parilla, and MJ Heben, *Proceedings of the 2000 DOE/NREL Hydrogen Program Review*, 8–10 (2000).
16. B Panella, M Hirscher, and S Roth, *Carbon*, **43**(10) (2005) 2209.
17. A Dillon, KM Jones, TA Bekkedahl, CH Kiang, DS Bethune, and MJ Heben, *Nature*, **386**(6623) (1997) 377.
18. C Wang, X Pang, G Wang, L Gao, and F Fu, *Photochem*, **3**(1) (2023) 15.
19. R Ströbel, J Garche, PT Moseley, L Jörissen, and G Wolf, *Journal of Power Sources*, **159**(2) (2006) 781.
20. K Atkinson, S Roth, M Hirscher, and W Grünwald, *Fuel Cells Bulletin*, **4**(38) (2001) 9.

21. C Liu, YY Fan, M Liu, HT Cong, HM Cheng, and MS Dresselhaus, *Science*, **286**(5442) (1999) 1127.
22. FL Darkrim, P Malbrunot, and GP Tartaglia, *International Journal of Hydrogen Energy*, **27**(2) (2002) 193.
23. A Reyhani, SZ Mortazavi, S Mirershadi, AZ Moshfegh, P Parvin, and AN Golikand, *Journal of Physical Chemistry C*, **115**(14) (2011) 6994.
24. A Dhanya, N Ranjan, and S Ramaprabhu, *Energy Storage*, **5**(4) (2023) e421.
25. M Aghababaei, AA Ghoreyshi, and K Esfandiari, *International Journal of Hydrogen Energy*, **45**(43) (2020) 23112.
26. R Zacharia, SU. Rather, SW Hwang, and KS Nahm, *Chemical Physics Letters*, **434**(4–6) (2007) 286.
27. T Yildirim, and S Ciraci, *Physical Review Letters*, **94**(17) (2005) 175501.
28. T Yildirim, J Íñiguez, and S Ciraci, *Physical Review B*, **72**(15) (2005) 153403.
29. L Gao, E Yoo, J Nakamura, W Zhang, and HT Chua, *Carbon*, **48**(11) (2010) 3250.
30. A D'Angola, G Colonna, and E Kustova, *Frontiers in Physics*, **10** (2022) 39.
31. M Babaie, I Bakoji, R Erfani, and A Nourian, *EGU General Assembly Conference Abstracts* (2021).
32. W Li, M Cao, S Meng, Z Li, H Xu, L Liu, and H Song, *Journal of Cleaner Production*, **387** (2023) 135913.
33. I Aminu, MA Nahil, and PT Williams, *Energy & Fuels*, **36**(7) (2022) 3788.
34. S Varshoy, B Khoshnevisan, M Mohammadi, and M Behpour, *Physica B: Condensed Matter*, **526** (2017) 143.
35. S Tsang, P Harris, and M Green, *Nature*, **362**(6420) (1993) 520.
36. A Kuznetsova, Jr JT Yates, VV Simonyan, JK Johnson, CB Huffman, and RE Smalley, *Chemical Physics Letters*, **115**(14) (2001) 6691.
37. A Kuznetsova, I Popova, Jr JT Yates, MJ Bronikowski, CB Huffman, J Liu, RE Smalley, HH Hwu, and JG Chen, *Journal of the American Chemical Society*, **123**(43) (2001)10699.
38. W Lee, SB Lee, JW Yi, BS Kim, and JH Byun, *Electrochemical and Solid-State Letters*, **14**(7) (2011) K37.
39. M Uysal, T Cetinkaya, M Kartal, A Alp, and H Akbulut, *Thin Solid Films*, **572** (2014) 216.
40. M Mohammadi and B Khoshnevisan, *International Journal of Hydrogen Energy*, **41**(24) (2016)10311.
41. E Pajootan, M Ye, M Zhang, S Niroumandrad, S Omanovic, and S Coulombe, *Journal of Physics D: Applied Physics*, **55**(19) (2022) 194001.
42. J Burress, M Kraus, M Beckner, R Cepel, G Suppes, C Wexler, P Pfeifer, *Nanotechnology*, **20**(20) (2009) 204026.
43. S Patchkovskii, JS Tse, SN Yurchenko, L Zhechkov, T Heine, and G Seifert, *Proceedings of the National Academy of Sciences*, **102**(30) (2005) 10439.
44. Y Ferro, F Marinelli, A Allouche, and C Brosset, *Journal of Chemical Physics*, **118**(12) (2003) 5650.
45. B Tarabová, P Lukeš, MU Hammer, H Jablonowski, T von Woedtke, S Reuter, and Z Machala, *Physical Chemistry Chemical Physics*, **21**(17) (2019) 8883.
46. W A Pryor, *Annual Review of Physiology*, **48**(1) (1986) 657.
47. P Lukes, E Dolezalova, I Sisrova, and M Clupek, *Plasma Sources Science and Technology*, **23**(1) (2014) 015019.
48. WH Glaze, JW Kang, and DH Chapin, *Hydrogen Peroxide and Ultraviolet Radiation* (1987) 335.
49. KF Sergeichev, NA Lukina, RM Sarimov, IG Smirnov, AV Simakin, AS Dorokhov, and SV Gudkov, *Frontiers in Physics*, **8** (2021) 614684.
50. JH Liang, TX Hu, D Wu, and ZM Sheng, *Physical Review E*, 105(4) (2022) 045206.
51. CY Hou, TK Kong, CM Lin, and HL Chen, *Applied Sciences*, **11**(11) (2021) 5304.
52. W Li, Y Bai, Y Zhang, M Sun, R Cheng, X Xu, Y Chen, and Y Mo, *Synthetic Metals*, **155**(3) (2005) 509.
53. D Sridhar, H Yu, JL Meunier, and S Omanovic, *Materials Advances*, **1**(2) (2020) 215.
54. D Sridhar, JL Meunier, and S Omanovic, *Materials Chemistry and Physics*, **223** (2019) 434.
55. A Ilnicka, M Skorupska, M Szkoda, Z Zarach, P Kamedulski, W Zielinski, and JP Lukaszewicz, *Scientific Reports*, **11**(1) (2021) 18387.
56. R Monsef, M Ghiyasiyan-Arani, and M Salavati-Niasari, *ACS Applied Energy Materials*, **4**(1) (2021) 680.